Journal of Science and Technology in Civil Engineering NUCE 2020. 14 (1): 65–76

A COMPUTATIONAL HOMOGENIZATION ANALYSIS OF MATERIALS USING THE STABILIZED MESH-FREE METHOD BASED ON THE RADIAL BASIS FUNCTIONS

Ho Le Huy Phuc[a,b,*], Le Van Canh[a], Phan Duc Hung[b]

[a]*Department of Civil Engineering, International University, VNU-HCMC, Quarter 6, Thu Duc district, Vietnam*
[b]*Faculty of Civil Engineering, Ho Chi Minh City University of Technology and Education, No 1 Vo Van Ngan street, Thu Duc district, Ho Chi Minh city, Vietnam*

Article history:
Received 05/08/2019, Revised 20/11/2019, Accepted 28/11/2019

Abstract

This study presents a novel application of mesh-free method using the smoothed-radial basis functions for the computational homogenization analysis of materials. The displacement field corresponding to the scattered nodes within the representative volume element (RVE) is split into two parts including mean term and fluctuation term, and then the fluctuation one is approximated using the integrated radial basis function (iRBF) method. Due to the use of the stabilized conforming nodal integration (SCNI) technique, the strain rate is smoothed at discrete nodes; therefore, all constrains in resulting problems are enforced at nodes directly. Taking advantage of the shape function which satisfies Kronecker-delta property, the periodic boundary conditions well-known as the most appropriate procedure for RVE are similarly imposed as in the finite element method. Several numerical examples are investigated to observe the computational aspect of iRBF procedure. The good agreement of the results in comparison with those reported in other studies demonstrates the accuracy and reliability of proposed approach.

Keywords: homogenization analysis; mesh-free method; radial point interpolation method; SCNI scheme.

https://doi.org/10.31814/stce.nuce2020-14(1)-06

1. Introduction

Almost materials in nature can be considered as inhomogeneous structures composed by different components. Predicting of the physical behavior of materials plays an important role in estimating the loading-capacity of structures. Therefore, it is necessary to develop the robust approaches for analysis of heterogeneous materials. Multiscale procedures are well-known as such efficient tools for this problem. An equivalent homogeneous material relied the RVE is used for a substitution of the heterogeneous one, and the problem is solved via the transition between micro-scale features and macro-response. The fundamental theories of homogeneous computation were early developed in the studies [1–10]. Then, the numerical implementation was concerned for improving the computational aspect of this method. A number of studies using different procedures, such as finite element method [11–14], boundary element method [15], mesh-free methods [16, 17] were published. This study

*Corresponding author. *E-mail address:* hlhphuc@hcmiu.edu.vn (Phuc, H. L. H.)

employs a mesh-free method based on the radial basis functions (RBF). A well-known disadvantage of meshless methods is lack of Kronecker-delta property in the shape function leading to the difficulty in imposing the essential boundary conditions. In the purpose of overcoming this issue, the so-called the point interpolation method (PIM) using polynomial basis function and radial point interpolation method (RPIM) using radial basis function were introduced [18]. Then, the low-order polynomial in combination with RBFs was also proposed for improving the accuracy and stability of RPIM. Furthermore, some models of PIM using smoothing technique based on nodes (NS-PIM), cells (CS-PIM) or edges (ES-PIM) were also developed in recent years, and more details can be found in [18, 19].

In this study, the stabilized conforming nodal integration (SCNI) scheme introduced by [20] is extended to RPIM, and the smoothed strains at every collocation point within the computational domain can be obtained. All constrains and conditions of problems will be imposed directly at the scattered nodes utilizing nodal integration procedure instead of using Gaussian quadrature, that reduces number of variables and integration points significantly. The numerical implementation is carried out to investigate the computational aspect, and the good agreement in comparison with other studies demonstrates the efficiency of proposed method.

2. Brief of homogenization theory

In this analysis, materials are considered to be macroscopically homogeneous, but microscopically heterogeneous. A heterogeneous body $V \in \mathbb{R}^3$ is replaced by an equivalent homogeneous one $V_M \in \mathbb{R}^3$. Next, a heterogeneous micro-base cell $V_m \in \mathbb{R}^3$ so-called the representative volume element (RVE) will be investigated at every material point $\mathbf{x} \in V_M$. The micro-structure is subjected to the body force $\mathbf{g}$, the surface load $\mathbf{t}$ on the static boundary Γ_t and constrained by the displacement field $\mathbf{u}$ on the kinematic boundary Γ_u.

The material response of macro-structure is determined by solving the macro-micro transitions problems, where the RVE size plays an important role. The RVE size must be significantly great to describe the material properties, but significantly small to ensure the reduced conditions of the transitions. Actually, the size of microscopic base cell is very small compared with the macro-scale ($l_m \ll l_M$); therefore, the body force $\mathbf{g}$ can be neglected in the micro-scale problem. The RVE equilibrium state can be formulated in absence of body forces as

$$\nabla \sigma_m = 0 \quad \text{in } V_m \tag{1}$$

where σ_m denotes the microscopic stress.

The micro-scale problem can be handled as the boundary value one in solid mechanics. The macroscopic strain ε_M are transferred to micro-structure in form of kinematic boundary constrains. The displacement field $\mathbf{u}$ consists two components involving mean part $\bar{\mathbf{u}}$ and fluctuation part $\tilde{\mathbf{u}}$

$$\mathbf{u} = \bar{\mathbf{u}} + \tilde{\mathbf{u}} = \varepsilon_M \mathbf{X} + \tilde{\mathbf{u}} \tag{2}$$

with $\mathbf{X}$ is the positional matrix of each material point in the computational domain.

Various approaches corresponding to different ways to impose the boundary condition have proposed in the literature, see [7, 13, 21]. This study uses the the most efficient in terms of convergence rate so-called periodic boundary condition. There are the periodicity of fluctuation field and anti-periodicity of traction field at RVE boundary

$$\tilde{\mathbf{u}}^+ = \tilde{\mathbf{u}}^- \quad \text{on } \Gamma_u; \quad \mathbf{t}^+ = -\mathbf{t}^- \quad \text{on } \Gamma_t \tag{3}$$

where $\tilde{\mathbf{u}}^+$ and $\tilde{\mathbf{u}}^-$ are the fluctuation field, $\mathbf{t}^+$ and $\mathbf{t}^-$ are the traction field of positive and negative boundaries, respectively.

The periodic boundary condition can be generally performed as

$$\mathbf{u}^+ - \mathbf{u}^- = \varepsilon_M(\mathbf{X}^+ - \mathbf{X}^-) \tag{4}$$

Note that, the boundary condition must always satisfy the averaging principle which is used to solve the couple of microscopic and macroscopic problem, see [1, 2, 10]. The macroscopic strain and stress tensors are computed by the volume average of microscopic those

$$\varepsilon_M = \frac{1}{V_m}\int_{V_m} \varepsilon_m dV_m; \qquad \sigma_M = \frac{1}{V_m}\int_{V_m} \sigma_m dV_m \tag{5}$$

Utilizing the formula $\nabla\mathbf{X} = \mathbf{I}$, the microscopic stress can be now expressed in the following relation

$$\sigma_m = (\nabla\sigma_m)\mathbf{X} + (\nabla\mathbf{X})\sigma_m = \nabla(\sigma_m\mathbf{X}) \tag{6}$$

Substituting Eq. (6) to Eq. (5) and applying the Green's theorem for integration, we obtain

$$\sigma_M = \frac{1}{V_m}\int_{V_m} \nabla(\sigma_m\mathbf{X})dV_m = \frac{1}{V_m}\int_{\Gamma_m} \mathbf{n}\sigma_m\mathbf{X}d\Gamma_m = \frac{1}{V_m}\int_{\Gamma_m} \mathbf{t}\mathbf{X}d\Gamma_m \tag{7}$$

Similarly, the strain averaging can be rewritten as

$$\varepsilon_M = \frac{1}{V_m}\int_{V_m} \nabla(\varepsilon_m\mathbf{X})dV_m = \frac{1}{V_m}\int_{\Gamma_m} \mathbf{n}\bar{\mathbf{u}}d\Gamma_m \tag{8}$$

The boundary condition must be defined to satisfy the constrain on the fluctuation field

$$\frac{1}{V_m}\int_{\Gamma_m} \mathbf{n}\tilde{\mathbf{u}}d\Gamma_m = 0 \tag{9}$$

Therefore, Eq. (8) can be rewritten as follow

$$\varepsilon_M = \frac{1}{V_m}\int_{\Gamma_m} \mathbf{n}\bar{\mathbf{u}}d\Gamma_m + \frac{1}{V_m}\int_{\Gamma_m} \mathbf{n}\tilde{\mathbf{u}}d\Gamma_m = \frac{1}{V_m}\int_{\Gamma_m} \mathbf{n}\mathbf{u}d\Gamma_m \tag{10}$$

The material constant matrix $\mathbf{D}_M$ for elastic state of macroscopic scale can be recalculated via the Hooke's law as

$$\sigma_M = \mathbf{D}_M\varepsilon_M \tag{11}$$

3. Point interpolation method using radial basis functions

Consider a scattered node $\mathbf{x}_Q^T = [x_1, x_2, ..., x_N]$ within a closed area Ω. In the original formulation of RPIM, the approximate function $u^h(\mathbf{x})$ is obtained by interpolating pass through the nodal value as

$$u^h(\mathbf{x}) = \mathbf{R}(\mathbf{x})\mathbf{a}(\mathbf{x}_Q) \tag{12}$$

where $\mathbf{a}(\mathbf{x}_Q)$ denotes the coefficient vector corresponding to the given point $\mathbf{x}_Q$; $\mathbf{R}(\mathbf{x})$ is the basis function vector which is expressed by

$$\mathbf{R}(\mathbf{x}) = [R_1(\mathbf{x}), R_2(\mathbf{x}), ..., R_N(\mathbf{x})] \tag{13}$$

with N is number of scattered points in the problem domain.

Following [18], the major advantage of RPIM is that the matrix $\mathbf{R}_Q$ is always invertable for arbitrary scattered nodes. However, the unexpected results in terms of accuracy may occur. Therefore, a polynomial term is added into the basis function to improve the computational efficiency. Additionally, using polynomial reproduction leads to the flexible selection of shape parameters. The approximate function for a set of points within the support domain is expressed as

$$u^h(\mathbf{x}) = \mathbf{R}(\mathbf{x})\mathbf{a} + \mathbf{p}(\mathbf{x})\mathbf{b} \tag{14}$$

where $\mathbf{a}$ and $\mathbf{b}$ are the coefficient vectors corresponding to radial basis function $\mathbf{R}(\mathbf{x})$ and polynomial basis function $\mathbf{p}(\mathbf{x})$, respectively

$$\mathbf{a}^T = \{a_1, a_2, ..., a_N\}; \quad \mathbf{b}^T = \{b_1, b_2, ..., b_M\} \tag{15}$$

with M is number of terms in $\mathbf{b}$ depending on the order of polynomial basis function.

Enforcing $u^h(\mathbf{x})$ function to pass through the scattered points within support domain, the matrix form of Eq. (14) is obtained by enforcing $u^h(\mathbf{x})$ function at every points as follows

$$\mathbf{U} = \mathbf{R}_Q\mathbf{a} + \mathbf{P}_M\mathbf{b} \tag{16}$$

where $\mathbf{R}_Q$ is given by

$$\mathbf{R}_Q = \begin{bmatrix} \cdots & \cdots & \cdots & \cdots \\ R_1(r_k) & R_2(r_k) & \cdots & R_N(r_k) \\ \cdots & \cdots & \cdots & \cdots \end{bmatrix}_{N\times N} \tag{17}$$

with $r_k = \| \mathbf{x}_k - \mathbf{x}_I \|$ is the distance between node I^{th} and point $\mathbf{x}_k$. The best ranked function in terms of accuracy named multi-quadric (MQ) is employed in this study

$$R_I(r_k) = (r_k^2 + c_I^2)^q \tag{18}$$

where $c_I = \alpha d_I$ is the shape parameter with $\alpha > 0$ and d_I is the minimal distance from point $\mathbf{x}_I$ to its neighbors.

To guarantee the unique approximation of function, the polynomial part must satisfy the extra requirement [18] and the following constrains are usually imposed

$$\mathbf{P}_M^T\mathbf{a} = 0 \tag{19}$$

The combination of Eqs. (16) and (19) gives

$$\begin{bmatrix} \mathbf{R}_Q & \mathbf{P}_M \\ \mathbf{P}_M^T & \mathbf{0} \end{bmatrix} \begin{Bmatrix} \mathbf{a} \\ \mathbf{b} \end{Bmatrix} = \begin{Bmatrix} \mathbf{U} \\ \mathbf{0} \end{Bmatrix} \tag{20}$$

Eq. (20) can be rewritten as

$$\mathbf{G} \begin{Bmatrix} \mathbf{a} \\ \mathbf{b} \end{Bmatrix} = \begin{Bmatrix} \mathbf{U} \\ \mathbf{0} \end{Bmatrix} \tag{21}$$

The coefficient vectors $\mathbf{a}$ and $\mathbf{b}$ can be computed by inverting matrix $\mathbf{G}$ and then substitute into Eq. (21). For convenience, a more efficient procedure proposed by [18] is employed

$$\mathbf{a} = \mathbf{R}_Q^{-1}\mathbf{U} - \mathbf{R}_Q^{-1}\mathbf{P}_M\mathbf{b}; \quad \mathbf{b} = \chi_b\mathbf{U} \tag{22}$$

where

$$\mathbf{b} = \chi_b \mathbf{U}; \quad \chi_b = [\mathbf{P}_M^T \mathbf{R}_Q^{-1} \mathbf{P}_M]^{-1} \mathbf{P}_M^T \mathbf{R}_Q^{-1} \tag{23}$$

Substituting **b** in Eq. (23) to in Eq. (22), we obtain

$$\mathbf{a} = \chi_a \mathbf{U} \tag{24}$$

where

$$\chi_a = \mathbf{R}_Q^{-1}[1 - \mathbf{P}_M \chi_b] = \mathbf{R}_Q^{-1} - \mathbf{R}_Q^{-1} \mathbf{P}_M \chi_b \tag{25}$$

Finally, the approximation function in Eq. (14) can be rewritten as

$$u^h(\mathbf{x}) = [\mathbf{R}(\mathbf{x})\chi_a + \mathbf{p}(\mathbf{x})\chi_b]\mathbf{U} = \sum_{I=1}^{N} \Phi_I(\mathbf{x}) u_I \tag{26}$$

The shape function and its partial derivatives for node k^{th} can be expressed as

$$\Phi_k = \sum_{I=1}^{N} R_I \chi_{Ik}^a + \sum_{J=1}^{M} p_J \chi_{Jk}^b \tag{27}$$

$$\frac{\partial \Phi_k}{\partial x} = \sum_{I=1}^{N} \frac{\partial R_I}{\partial x} \chi_{Ik}^a + \sum_{J=1}^{M} \frac{\partial p_J}{\partial x} \chi_{Jk}^b; \quad \frac{\partial \Phi_k}{\partial y} = \sum_{I=1}^{N} \frac{\partial R_I}{\partial y} \chi_{Ik}^a + \sum_{J=1}^{M} \frac{\partial p_J}{\partial y} \chi_{Jk}^b \tag{28}$$

For purpose of computational improvement, this study employs the strain smoothing method proposed in [20] for use in nodal integration schemes as

$$\tilde{\varepsilon}_{ij}^h(\mathbf{x}_J) = \frac{1}{a_J} \int_{\Omega_J} \frac{1}{2}(u_{i,j}^h + u_{j,i}^h) \mathrm{d}\Omega = \frac{1}{2a_J} \oint_{\Gamma_J} \left(u_i^h n_j + u_j^h n_i \right) \mathrm{d}\Omega \tag{29}$$

where $\tilde{\varepsilon}_{ij}^h$ is the smoothed value of strains ε_{ij}^h at node J; a_J and Γ_J are the area of the representative domain Ω_J of node J, respectively.

The smooth version of the strains can be expressed as

$$\varepsilon^h(\mathbf{x}_J) = \left[\begin{array}{ccc} \tilde{\varepsilon}_{xx}^h(\mathbf{x}_J) & \tilde{\varepsilon}_{yy}^h(\mathbf{x}_J) & 2\tilde{\varepsilon}_{xy}^h(\mathbf{x}_J) \end{array} \right]^T = \tilde{\mathbf{B}}\mathbf{d} \tag{30}$$

where **d** denotes the displacement vector and $\tilde{\mathbf{B}}$ is the strain matrix whose components are calculated using the derivatives of shape function as

$$\tilde{\Phi}_{I,\alpha}(\mathbf{x}_J) = \frac{1}{a_J} \oint_{\Gamma_J} \Phi_I(\mathbf{x}_J) n_\alpha(\mathbf{x}) \mathrm{d}\Gamma = \frac{1}{2a_J} \sum_{k=1}^{ns} \left(n_\alpha^k \; l^k + n_\alpha^{k+1} \; l^{k+1} \right) \Phi_I(\mathbf{x}_J^{k+1}) \tag{31}$$

where $\tilde{\Phi}$ is the smoothed version of Φ; ns is the number of segments of a Voronoi nodal domain Ω_J in the Fig. 1; $\mathbf{x}_J^k$ and $\mathbf{x}_J^{k+1}$ are the coordinates of the two end points of boundary segment Γ_J^k which has length l^k and outward surface normal n^k.

It is interested to note that the shape function of RPIM possesses Kronecker delta property. Consequently, the essential boundary conditions can be enforced by the similar way as in the finite element method. Furthermore, the stabilized shape function also yields to the reduction of computational cost.

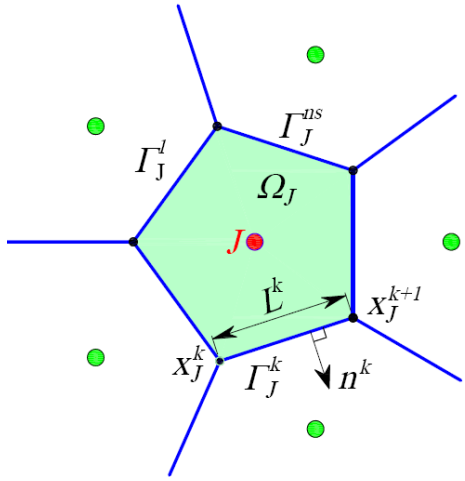

Figure 1. Geometry definition of a representative nodal domain

4. RPIM discretisation of the homogenization problems

The displacement field $\mathbf{u}$ are approximated in terms of nodal reflection within the problem domain using the RPIM procedure as follow

$$u^h(\mathbf{x}) = \sum_{I=1}^{N} \Phi_I(\mathbf{x})\mathbf{u}_I = \sum_{I=1}^{N} \Phi_I(\mathbf{x}) \begin{bmatrix} u_I \\ v_I \end{bmatrix} \tag{32}$$

where u_I and v_I are the nodal displacement components corresponding to node I^{th}; N is number nodes in the computational domain of area Ω_m.

The periodic constrain in Eq. (6) can be recalled and expressed as follow

$$\mathbf{u}^+ - \mathbf{u}^- = \mathbf{u}^A - \mathbf{u}^B \tag{33}$$

where $\mathbf{u}^A$ and $\mathbf{u}^B$ are the displacement of nodes at the RVE corners.

Denoting $\mathbf{C}$ for the coefficient matrix containing the $(0,\ 1,\ -1)$ values, Eq. (33) can be performed as

$$\mathbf{C}\mathbf{u} = 0 \tag{34}$$

The displacement vector $\mathbf{u} = [u_1,\ v_1,\ ...,\ u_N,\ v_N]^T$ is determined from the equation system, in which the global stiffness matrix $\mathbf{K}$ is built by assembling 2×2 matrices $\mathbf{K}_{IJ}$ defined by

$$\mathbf{K}_{IJ} = \int_{\Omega_m} \mathbf{B}_I^T \mathbf{D}_m \mathbf{B}_J d\Omega_m, \quad I, J = 1, 2, \ldots, N \tag{35}$$

where $\mathbf{D}_m$ is the material constant matrix of micro-scale.

The global load vector $\mathbf{f}$ consists 2×1 matrices $\mathbf{f}_I$ as

$$\mathbf{f}_I = \int_{\Gamma_t} \Phi_I \mathbf{t} d\Gamma_t, \quad I = 1, 2, \ldots, N \tag{36}$$

In this study, the condensation method is used to impose the boundary condition. The constrains of displacement degree of freedoms (DOFs) in Eq. (34) are rewritten as

$$\begin{bmatrix} \mathbf{C}_i & \mathbf{C}_d \end{bmatrix} \begin{bmatrix} \mathbf{u}_i \\ \mathbf{u}_d \end{bmatrix} = 0 \tag{37}$$

where $\mathbf{u}_i$ and $\mathbf{u}_d$ are the independent and dependent DOFs, respectively and

$$\mathbf{u}_d = -\mathbf{C}_d^{-1}\mathbf{C}_i\mathbf{u}_i = \mathbf{C}_{di}\mathbf{u}_i \tag{38}$$

Then, the linear equation system can be expressed as

$$\begin{bmatrix} \mathbf{K}_{ii} & \mathbf{K}_{id} \\ \mathbf{K}_{di} & \mathbf{K}_{dd} \end{bmatrix} \begin{bmatrix} \mathbf{u}_i \\ \mathbf{u}_d \end{bmatrix} = \begin{bmatrix} \mathbf{f}_i \\ \mathbf{f}_d \end{bmatrix} \tag{39}$$

In condensation method, the dependent DOFs $\mathbf{u}_d$ will be eliminated from the equation system. The reduced forms of the stiffness matrix $\mathbf{K}$ and loading vector $\mathbf{f}$ are now calculated as

$$\mathbf{K}^* = \mathbf{K}_{ii} + \mathbf{K}_{id}\mathbf{C}_{di} + \mathbf{C}_{di}^T\mathbf{K}_{di} + \mathbf{C}_{di}^T\mathbf{K}_{dd}\mathbf{C}_{di}; \quad \mathbf{f}^* = \mathbf{f}_i + \mathbf{C}_{di}^T\mathbf{f}_d \tag{40}$$

The equation system is rewritten as

$$\mathbf{K}^*\mathbf{u} = \mathbf{f}^* \quad \text{or} \quad \begin{bmatrix} \mathbf{K}_{aa} & \mathbf{K}_{ab} \\ \mathbf{K}_{ba} & \mathbf{K}_{bb} \end{bmatrix} \begin{bmatrix} \mathbf{u}_a \\ \mathbf{u}_b \end{bmatrix} = \begin{bmatrix} 0 \\ \mathbf{f}_b \end{bmatrix} \tag{41}$$

where a and b denote the inner nodes and corner nodes, respectively.

The displacement corresponding to the corner nodes I^{th} can be determined by

$$\mathbf{u}_{bI} = \begin{bmatrix} X & 0 & 0.5Y \\ 0 & Y & 0.5X \end{bmatrix} \begin{bmatrix} \varepsilon_{xx} \\ \varepsilon_{yy} \\ \varepsilon_{xy} \end{bmatrix} = \chi_{bI}\varepsilon_M \tag{42}$$

with (X, Y) is the coordinate of the corner nodes I^{th} in the problem domain.

Using the condensation method, the reduced equation system is performed via the corner DOFs as

$$\mathbf{K}_{bb}^*\mathbf{u}_b = \mathbf{f}_b^* \tag{43}$$

where

$$\mathbf{K}_{bb}^* = \mathbf{K}_{bb} - \mathbf{K}_{ba}\mathbf{K}_{aa}^{-1}\mathbf{K}_{ab} \tag{44}$$

The macroscopic stress satisfies the averaging principle

$$\sigma_M = \frac{1}{\Omega_m}\int_{\Gamma_m} \mathbf{t}\mathbf{X}d\Gamma_m = \frac{1}{\Omega_m}\chi_b^T\mathbf{f}_b^* = \frac{1}{\Omega_m}\chi_b^T\mathbf{K}_{bb}^*\mathbf{u}_b = \frac{1}{\Omega_m}\chi_b^T\mathbf{K}_{bb}^*\chi_b\varepsilon_M \tag{45}$$

Finally, homogenizing Eqs. (11) and (45), we obtain the material constant matrix for the macro-scale as

$$\mathbf{D}_M = \begin{bmatrix} D_{11} & D_{12} & 0 \\ D_{21} & D_{22} & 0 \\ 0 & 0 & D_{66} \end{bmatrix} = \frac{1}{\Omega_m}\chi_b^T\mathbf{K}_{bb}^*\chi_b \tag{46}$$

5. Numerical solutions

5.1. Material models with a central inclusion

The micro-structure with an inclusion of radius R at center is taken into account in this example. The geometry and dimension of RVE are illustrated in Fig. 2, all dimensions are in μm. The constituent of material model includes Epoxy matrix (E_m = 3.13 GPa, ν_m = 0.34) embedded with the Glass fiber (E_c = 73 GPa, ν_c = 0.2).

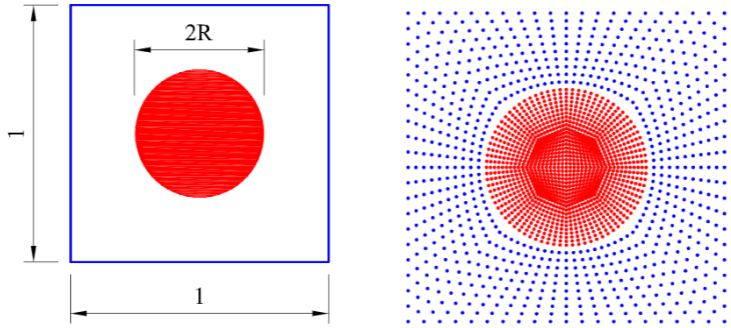

(a) Geometry and dimension (b) Nodal discretization

Figure 2. Microstructure with inclusion: geometry and discretization (V/V_0 = 20%)

Several volume ratios V/V_0 are investigated and the numerical solutions using RPIM and FEM models are collected in Table 1. From the table, it can be seen that RPIM results are very close to FEM models when using the same meshing database (2041 nodes, 2000 Q4-elements, 4000 T3-elements). The advantage of RPIM method is that number of integration points required to construct the stiffness matrix are much less than those in FEM formulations due to the use of SCNI technique leading to the integrations to be directly enforced at discretized nodes in the computational domain. That means the computational cost is significantly decreased using RPIM procedure.

Table 1. RVE with inclusion: material parameters

V/V_0	Approach	Material parameters (GPa)			
		D_{11}	D_{22}	D_{12}	D_{66}
10%	RPIM	3.951	3.951	1.308	1.308
	FEM-T3	4.102	4.102	1.341	1.364
	FEM-Q4	4.099	4.099	1.339	1.365
20%	RPIM	4.873	4.873	1.532	1.540
	FEM-T3	4.823	4.823	1.528	1.527
	FEM-Q4	4.820	4.820	1.527	1.528
30%	RPIM	5.892	5.892	1.691	1.776
	FEM-T3	5.776	5.776	1.748	1.687
	FEM-Q4	5.774	5.774	1.747	1.688
Number of integration points: RPIM: 2041; FEM-T3: 4000; FEM-Q4: 32000					

The effect shear modulus over the matrix modulus are compared with the analytical results reported in [22], the numerical solutions reported in [21] and present FEM models. The comparison is also plotted in Fig. 3(a). The agreement of present solutions and the analytical as well as other numerical models shows the reasonability of proposed method. The displacement and stress fields are shown in Figs. 3(b) and 3(c). It can be observed from the stress distribution that the stress is mainly concentrated at the kernel in where the Glass fiber is reinforced.

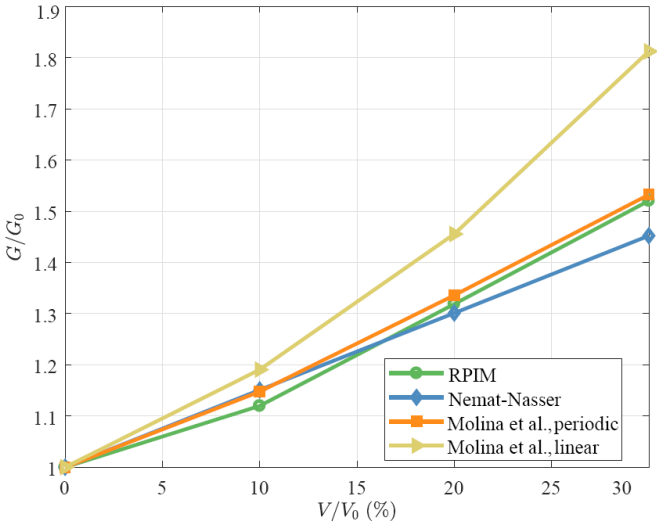

(a) Comparison of the effect shear modulus ratios G/G_0

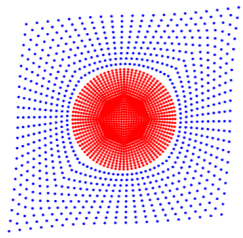

(b) Displacement field

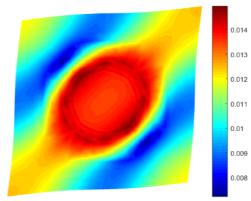

(c) Stress field

Figure 3. RVE with inclusion: the solutions

5.2. *Material models reinforced with the fibers*

The example investigates two representative material sections composed of aluminum matrix with Young's modulus E_m = 72.5 GPa and Poisson ratio ν_m = 0.33. The second material consisting short and long boron fibers with Young's modulus E_c = 400 GPa and Poisson's ratio ν_c = 0.2 are embedded in the matrix. Fig. 4 shows the dimensions (μm) and distribution of heterogeneity.

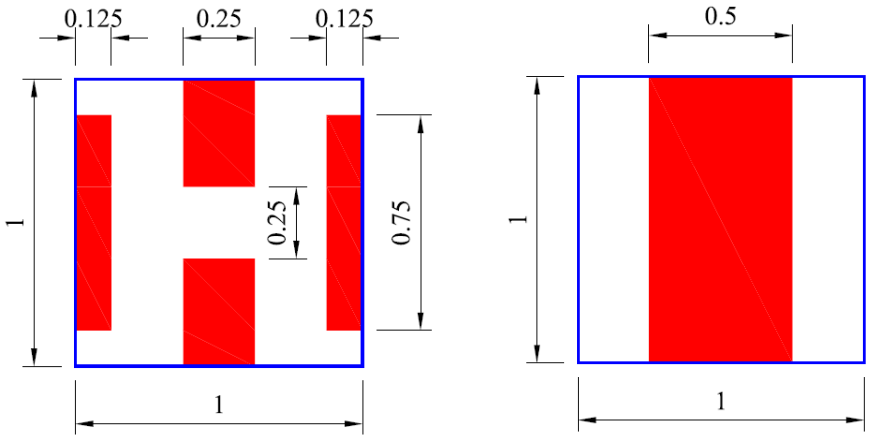

(a) RVE with short fiber

(b) RVE with long fiber

Figure 4. Micro-structure with rectangular heterogeneity

To demonstrate the accuracy and reliability of proposed method, the numerical results of material properties are compared with those using the global-local FEM analysis reported in [5], VCFEM and HOMO2D in [6]. From Tables 2 and 3, it can be observed that present procedure can prove the compatible solutions in comparison with numerical methods in [5, 6].

Table 2. The comparison of material properties in case of short fiber model

Author	Material properties (GPa)			
	D_{11}	D_{22}	D_{12}	D_{66}
Present RPIM	124.084	152.529	36.800	42.915
Fish and Wagimen [5]	122.357	151.351	36.191	42.112
Ghosh et al. [6], VCFEM	118.807	139.762	38.052	42.440
Ghosh et al. [6], HOMO2D	122.400	151.200	36.230	42.100

Table 3. The comparison of material properties in case of long fiber model

Author	Material properties (GPa)			
	D_{11}	D_{22}	D_{12}	D_{66}
Present RPIM	137.372	245.842	36.284	47.396
Fish and Wagimen [5]	136.147	245.810	36.076	46.850
Ghosh et al. [6], VCFEM	136.137	245.810	36.076	46.850
Ghosh et al. [6], HOMO2D	136.100	245.800	36.080	46.850

The displacement and the stress field distributions are plotted in Figs. 5 and 6. It can be seen that the stresses are concentrated at positions where the stiffness significantly increase owing to the reinforcement of the fibers.

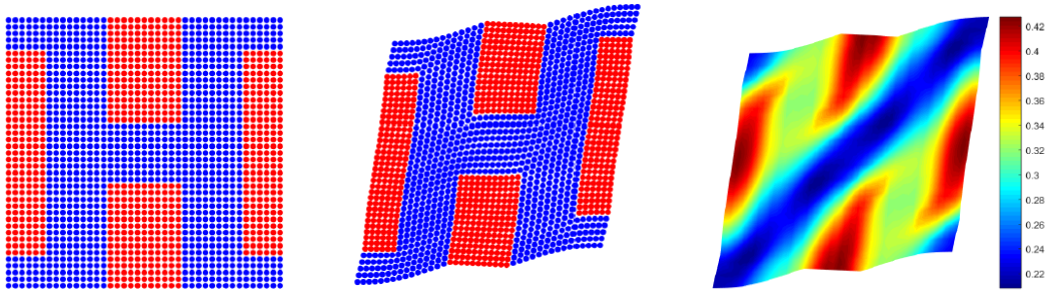

(a) RVE model (b) Displacement field (c) Stress field

Figure 5. Material reinforced with short fiber using RPIM method (1681 nodes)

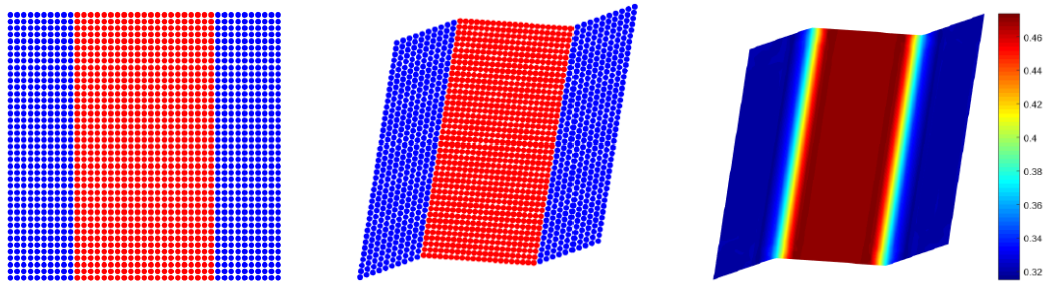

(a) RVE model (b) Displacement field (c) Stress field

Figure 6. Material reinforced with long fiber using RPIM method (1681 nodes)

6. Conclusions

A novel mesh-free method based on radial basis functions and SCNI scheme has been successfully applied for homogeneous analysis of materials. The important advantage of proposed method in comparison with mesh-based ones is the absence of the mesh and the high-order shape function, which may increase the accuracy and convergence rate of solutions. Forever, the periodic boundary condition for RVE is applied owing to the RPIM shape function possesses Kronecker-delta property. The SCNI scheme for calculation of strains helps all constrains be enforced directly at scattered nodes in the problem domain, and the computational cost can be reduced significantly. However, this study only aims to analyse the elastic behavior of materials; therefore, the future works will extend to the inelastic respond of materials and structures.

Acknowledgement

This research is funded by International University - Vietnam National University Ho Chi Minh City under grant number T2019-01-CE.

References

[1] Hill, R. (1963). Elastic properties of reinforced solids: some theoretical principles. *Journal of the Mechanics and Physics of Solids*, 11(5):357–372.

[2] Hill, R. (1984). On macroscopic effects of heterogeneity in elastoplastic media at finite strain. In *Mathematical Proceedings of the Cambridge Philosophical Society*, volume 95, Cambridge University Press, 481–494.

[3] Budiansky, B. (1965). On the elastic moduli of some heterogeneous materials. *Journal of the Mechanics and Physics of Solids*, 13(4):223–227.

[4] Hashin, Z., Wendt, F. W. (1970). Theory of composite materials. *Mechanics of Composite Materials*, 201–242.

[5] Fish, J., Wagiman, A. (1993). Multiscale finite element method for a periodic and nonperiodic heterogeneous medium. *ASME Applied Mechanics Division-publications-AMD*, 157:95–95.

[6] Ghosh, S., Lee, K., Moorthy, S. (1995). Multiple scale analysis of heterogeneous elastic structures using homogenization theory and Voronoi cell finite element method. *International Journal of Solids and Structures*, 32(1):27–62.

[7] Miehe, C. (1996). Numerical computation of algorithmic (consistent) tangent moduli in large-strain computational inelasticity. *Computer Methods in Applied Mechanics and Engineering*, 134(3-4):223–240.

[8] Moulinec, H., Suquet, P. (1998). A numerical method for computing the overall response of nonlinear composites with complex microstructure. *Computer Methods in Applied Mechanics and Engineering*, 157(1-2):69–94.

[9] Michel, J.-C., Moulinec, H., Suquet, P. (1999). Effective properties of composite materials with periodic microstructure: a computational approach. *Computer Methods in Applied Mechanics and Engineering*, 172(1-4):109–143.

[10] Nemat-Nasser, S. (1999). Averaging theorems in finite deformation plasticity. *Mechanics of Materials*, 31(8):493–523.

[11] Miehe, C., Koch, A. (2002). Computational micro-to-macro transitions of discretized microstructures undergoing small strains. *Archive of Applied Mechanics*, 72(4-5):300–317.

[12] Miehe, C. (2003). Computational micro-to-macro transitions for discretized micro-structures of heterogeneous materials at finite strains based on the minimization of averaged incremental energy. *Computer Methods in Applied Mechanics and Engineering*, 192(5-6):559–591.

[13] Kouznetsova, V., Brekelmans, W. A. M., Baaijens, F. P. T. (2001). An approach to micro-macro modeling of heterogeneous materials. *Computational Mechanics*, 27(1):37–48.

[14] Phuong, N. H., Canh, L. V., Kien, N. T. (2019). Determination of the effective properties of random orientation polycrystals using homogenization method. *Journal of Science and Technology in Civil Engineering (STCE)-NUCE*, 13(4V):129–138. (in Vietnamese).

[15] Sfantos, G. K., Aliabadi, M. H. (2007). Multi-scale boundary element modelling of material degradation and fracture. *Computer Methods in Applied Mechanics and Engineering*, 196(7):1310–1329.

[16] Ahmadi, I., Aghdam, M. M. (2011). A truly generalized plane strain meshless method for combined normal and shear loading of fibrous composites. *Engineering Analysis with Boundary Elements*, 35(3): 395–403.

[17] Li, L. Y., Wen, P. H., Aliabadi, M. H. (2011). Meshfree modeling and homogenization of 3D orthogonal woven composites. *Composites Science and Technology*, 71(15):1777–1788.

[18] Liu, G.-R. (2009). *Meshfree methods: moving beyond the finite element method*. CRC Press.

[19] Liu, G. R., Zhang, G. Y. (2013). *Smoothed point interpolation methods: G space theory and weakened weak forms*. World Scientific.

[20] Chen, J.-S., Wu, C.-T., Yoon, S., You, Y. (2001). A stabilized conforming nodal integration for Galerkin mesh-free methods. *International Journal for Numerical Methods in Engineering*, 50(2):435–466.

[21] Molina, A. J. C., de Souza Neto, E. A., Peric, D. (2005). Homogenized tangent moduli for heterogenous materials. In *Proceedings of the 13th UK National Conference of the Association of Computational Mechanics in Engineering*, Citeseer, 17–20.

[22] Nemat-Nasser, S., Hori, M. (2013). *Micromechanics: overall properties of heterogeneous materials*, volume 37. Elsevier.